THE EUROPEAN
PHYSICAL JOURNAL PLUS

Bounds on the absorptive parts of the chromomagnetic and chromoelectric dipole moments of the top quark from LHC data

A. I. Hernández-Juárez[1,a] , **A. Moyotl**[2,b], **G. Tavares-Velasco**[1,c]

[1] Facultad de Ciencias Físico-Matemáticas, Benemérita Universidad Autónoma de Puebla, C.P. 72570 Puebla, PUE, Mexico
[2] Ingeniería en Mecatrónica, Universidad Politécnica de Puebla, Tercer Carril del Ejido Serrano s/n, San Mateo Cuanalá, Juan C. Bonilla, Puebla, PUE, Mexico

Abstract Bounds on the absorptive (imaginary) parts of the top quark chromomagnetic $\hat{\mu}_t$ and chromoelectric $\hat{d}_t$ dipole moments are obtained by reinterpreting the most recent LHC data in top quark pair production. It is found that both limits are of the order of $10^{-1} - 10^{-2}$, which are consistent with the standard model prediction of $\text{Im}[\hat{\mu}_t]$. The effects of the absorptive parts of the top quark dipole moments are also studied via some kinematic distributions of $\bar{t}t$ production, though no significant deviation from the standard model leading-order contribution is observed. Our bounds can be useful to constrain the parameter space of standard model extensions.

1 Introduction

Quite recently, the study of the chromomagnetic dipole moment (CMDM) $\hat{\mu}_t$ of the top quark has become a topic of great interest both theoretically and experimentally. On the theoretical side, a new evaluation of the lowest order contributions to $\hat{\mu}_t$ within the framework of the standard model (SM) is presented in Refs. [1, 2], which has settled some ambiguities found in previous evaluations: in contrast to what was claimed before [3], it has become clear that the CMDM is infrared divergent, with the divergent part arising from the non-abelian term of the gluon field tensor [1, 2]. Therefore, the study of the static CMDM has no sense in perturbative QCD. Nevertheless, the off-shell CMDM is finite and gauge-independent in the SM [1], and therefore, it can be a valid observable quantity. In addition, several non-SM contributions to the CMDM have been calculated up to the one-loop level in the framework of extension theories such as two Higgs doublet models (THDM) [4], fourth-generation THDMs [5], 331 models [6], models with an extra Z gauge boson [7]. As far as the top quark chromoelectric dipole moment (CEDM) $\hat{d}_t$ is concerned, it is induced up to the three-loop level in the SM [8] and thus could give a clear signal of *CP* violation. The top quark CEDM has also been a topic of in the literature as it can arise at one-loop level in some beyond the SM (BSM) theories [5, 6], thereby opening the possibility of a considerable enhancement. In general, both the off-shell CMDM and CEDM can have nonzero imaginary parts, whose effects remain almost unexplored.

On the experimental side, the leading-order corrections to the cross section of top quark pair production induced by the top quark CMDM and CEDM have been studied in [9–29], and the next-to-leading-order corrections have also been calculated more recently [30–32], whereas the effects of the dipole moments have been analyzed in some processes [33–46]. The CMS collaboration has imposed the following current bounds on the top quark CMDM and CEDM: $-0.014 < \hat{\mu}_t < 0.004$ and $-0.020 < \hat{d}_t < 0.012$ [47], which where obtained via two opposite sign leptons (e^+e^-, $e^\pm\mu^\mp$, $\mu^+\mu^-$) in the final state. Furthermore, the CMS collaboration also set the limits $\hat{\mu}_t = -0.024^{+0.013}_{-0.009}(\text{stat})^{+0.016}_{-0.011}(\text{syst})$ and $|\hat{d}_t| < 0.03$ [48] obtained by the analysis of lepton+jets events in the final state. These bounds were extracted from experimental data by assuming that the top quark CMDM and CEDM are real quantities.

An appropriate approach to study the anomalous couplings and their effects on observable processes in a model-independent way is provided by the effective Lagrangian approach, where a $SU(3)_c \times SU(2)_L \times U(1)_Y$ gauge-invariant effective Lagrangian is introduced to parametrize the effects of physics BSM. Such an effective Lagrangian contains the SM Lagrangian plus a tower of effective operators $\mathcal{O}^n$ ($n > 4$) constructed out of the SM fields

$$\mathcal{L}^{\text{Eff.}} = \mathcal{L}^{SM} + \sum_{n>0} \frac{\alpha_\mathcal{O}}{\Lambda^{n+4}} \mathcal{O}^{n+4}, \tag{1}$$

a e-mail: alaban7_3@hotmail.com (corresponding author)

b e-mail: agustin.moyotl@uppuebla.edu.mx

c e-mail: gtv@fcfm.buap.mx

Springer

where the coupling constants $\alpha_{\mathcal{O}}$ parametrize our ignorance of the new physics and Λ is the new physics scale. In particular, non-standard top-gluon interactions arise from a dimension-six operator [49, 50], which after electroweak symmetry breaking gives rise to the following Lagrangian

$$\mathcal{L} = -g_s \bar{t} T^a \left[\frac{\sigma^{\mu\nu}}{2m_t} \left(\hat{\mu}_t + i\hat{d}_t \gamma^5 \right) G^a_{\mu\nu} \right] t, \tag{2}$$

where T^a are the $SU(3)$ color generators, G^a_μ are the gluon fields, $G^a_{\mu\nu} = \partial_\mu G^a_\nu - \partial_\nu G^a_\mu - g_s f_{abc} G^b_\mu G^c_\nu$ is the gluon field tensor, whereas $\hat{\mu}_t$ and $\hat{d}_t$ are constant coefficients that parametrize the anomalous contributions to the $\bar{t}tg$ coupling arising from new physics. It must be noted, however, that the above Lagrangian does not yield the most general $\bar{t}tg$ interaction, which in fact can be written in terms of four independent form factors [51].

The above Lagrangian also describes the interaction between an off-shell gluon and two on-shell quarks [52]. Since the off-shell CMDM and CEDM of the top quark are complex in general, they will be written as

$$\hat{\mu}_t = \text{Re}\left[\hat{\mu}_t\right] + i\text{Im}\left[\hat{\mu}_t\right], \tag{3}$$

$$\hat{d}_t = \text{Re}\left[\hat{d}_t\right] + i\text{Im}\left[\hat{d}_t\right]. \tag{4}$$

As far as the SM predictions are concerned, the real and imaginary parts of the off-shell CMDM of the top quark are of the order of $10^{-2} - 10^{-3}$ [1], whereas the predictions for the off-shell CEDM are not available yet. Nevertheless, in BSM theories both real and imaginary parts of the off-shell top quark CEDM are of the order of 10^{-19} [6]. On the other hand, the effects of the absorptive parts of the CMDM and CEDM at LHC were first studied in [23], but to our knowledge, there is no update on such analysis, which we believe is in the order given the current experimental bounds on these observables.
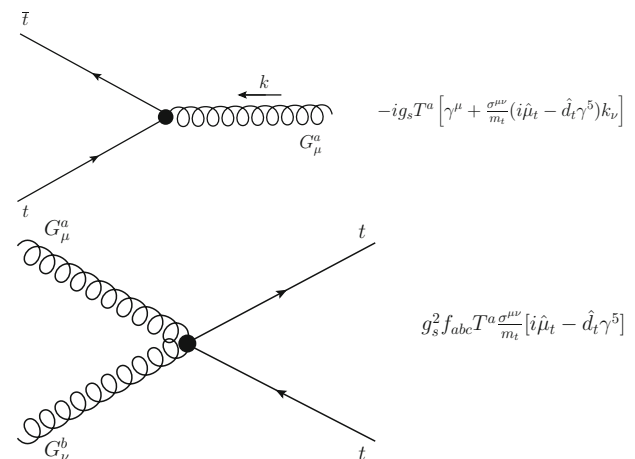
We would like to note that although the off-shell dipole form factors are dependent on the gluon transfer momentum, we will follow the authors of Ref. [23] and consider in our analysis below that both the real and absorptive parts of the dipole form factors are constant, which is valid as long as unitarity is not spoiled. This approach has also been used, for instance, to obtain bounds on the trilinear neutral gauge boson couplings $Z\gamma V^* \; (V = \gamma, Z)$ [53], which due to Bose statistics and angular momentum conservation are non-vanishing only for off-shell V. In fact, over a large interval of q^2, the SM contribution to the top quark CMDM shows little variation [1], and the same is true for both the CMDM and CEDM in some BSM theories (see for instance [6, 7]). Our main goal is to obtain bounds on $\text{Im}\left[\hat{\mu}_t\right]$ and $\text{Im}\left[\hat{d}_t\right]$ using the data for top quark pair production at the LHC run 2, which in turn can be useful to constraint the parameter space of some BSM theories.

Our work is organized as follows: In Sect. 2, we discuss the framework for the study of the CMDM and CEDM absorptive parts. Section 3 presents a novel calculation of the parton cross sections of $t\bar{t}$ production for complex CMDM and CEDM, which to our knowledge has not been reported before. In Sect. 4, a numerical simulation is presented for top quark pair production at the LHC via MadGraph5, where the effective Lagrangian of Eq. (2) was implemented with the help of the FeynRules package. The results for the $t\bar{t}$ cross section as a function of the real and imaginary parts of $\hat{\mu}_t$ and $\hat{d}_t$ are then used to obtain bounds on their absorptive parts. The possibility that kinematic distributions could be helpful to disentangle the top quark CMDM and CEDM absorptive parts is examined in Sect. 5. Finally, in Sect. 6 we present our conclusions.

2 Remarks on the absorptive parts of the CMDM in the SM

In the SM, the CMDM of quarks arises at the one-loop level through the Feynman diagrams of Figs. 1 (QCD contribution) and 2 (electroweak contribution). The off-shell CMDM $\hat{\mu}_q(q^2)$ can develop an absorptive (imaginary) part when the gluon transfer four-momentum $\hat{q} = \sqrt{q^2}$ crosses the threshold $\hat{q} \geq 2m$, with m the mass of the virtual particles attached to the off-shell gluon. In such region, these particles are allowed to be pair produced, which is true for all energies of the external gluon in Feynman diagram (b) of Fig. 1, whereas the threshold is $\hat{q} \geq 2m_q$ for Feynman diagrams 1a and 2a, c, and $\hat{q} \geq 2m_{q'}$ in Feynman diagram 2b. The absorptive contributions to the CMDM can also be extracted by the Cutkosky rules [54], which yield the same results obtained via the usual techniques for Feynman diagram calculation [55]. It is also important to emphasize that the SM contribution to the off-shell dipole moment $\hat{\mu}_q(q^2)$ is finite and gauge-independent for arbitrary q^2.

For the top quark CMDM, the contribution from the diagram (b) of Fig. 2 develops an absorptive part at $\hat{q} = 2m_b$, whereas that from the diagram (b) of Fig. 1 is complex for any $\hat{q}$ value. The remaining contributions become complex at $\hat{q} = 2m_t$. Moreover, the corresponding contributions to the top quark CEDM would also become complex at the same energy thresholds. It is thus interesting to obtain a bound on the absorptive part of the top quark CMDM and CEDM consistent with the CMS limits. Such a bound can be interpreted as a limit on the new physics effects inducing new contributions to the CMDM and CEDM of the top quark. To assess the order of magnitude of the absorptive part of the CMDM at the LHC energies, we have performed a numerical evaluation of the analytical expressions of Ref. [1] to find the energy interval of the transfer momentum of the gluon where the real part of the top quark CMDM predicted by the SM matches the CMS bounds [47, 48]. We obtain that the value $\text{Re}\left[\hat{\mu}_t\right] = -0.024$ reported in Ref [48] corresponds to the 57 GeV$\leqslant \hat{q} \leqslant$ 59 GeV interval, where the respective absorptive part value is $\text{Im}\left[\hat{\mu}_t\right] \approx -0.034$. As far as the bound $-0.014 < \text{Re}\left[\hat{\mu}_t\right] < 0.004$ reported in Ref. [47], it is consistent with energies above $\hat{q} = 85$ GeV, in this case, the

Fig. 1 QCD contributions to the CMDM of quarks in the SM

(a)   **(b)**

(a)   **(b)**   **(c)**
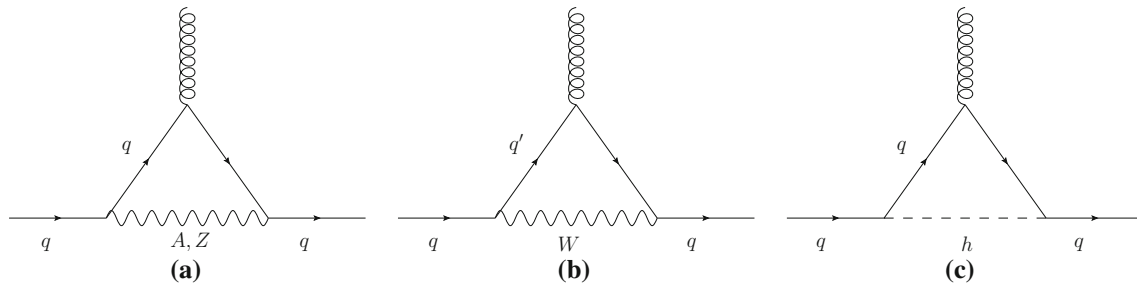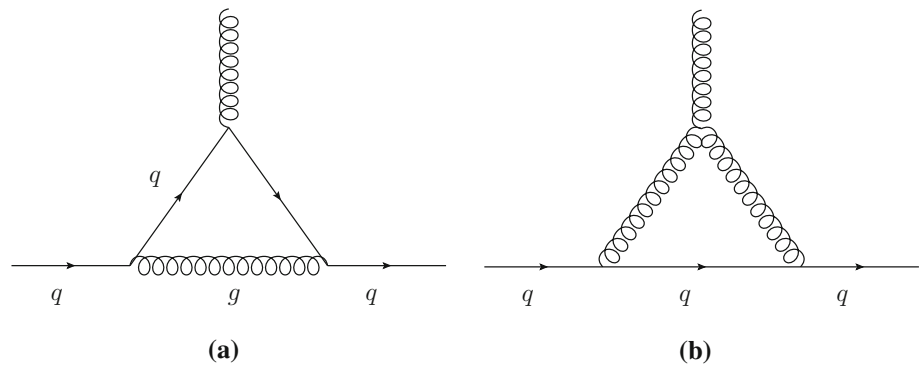
Fig. 2 Electroweak contributions to the CMDM of quarks in the SM

Fig. 3 Feynman rules for the anomalous $\bar{t}tg$ and $\bar{t}tgg$ couplings arising from Lagrangian (2).

$$-ig_s T^a \left[\gamma^\mu + \frac{\sigma^{\mu\nu}}{m_t}(i\hat{\mu}_t - \hat{d}_t \gamma^5)k_\nu \right]$$

$$g_s^2 f_{abc} T^a \frac{\sigma^{\mu\nu}}{m_t}[i\hat{\mu}_t - \hat{d}_t \gamma^5]$$

absorptive part can be one order of magnitude smaller than in the previous one: for values around $\hat{q} = 85$ GeV, $\text{Im}[\hat{\mu}_t] \approx -0.028$, whereas at higher energies the corresponding value is of the order of 10^{-3} and remains almost constant as the energy increases.

3 Contributions of CMDM and CEDM to $t\bar{t}$ production

Top pair production can receive contributions from the anomalous $\bar{t}tg$ coupling [11, 12] of Eq. (2) but also from the non-SM $\bar{t}tgg$ vertex arising from the non-abelian part of the gluon field strength tensor. The corresponding Feynman rules follow straightforwardly and are shown in Fig. 3. As already mentioned, in a strict sense, the top quark dipole form factors are functions of the gluon transfer momentum q^2, with such functions being model dependent. Furthermore, when working with off-shell green functions one must address the problem of gauge dependence. Along this line, methods such as the pinch technique have been used in the past to remove any gauge-dependent terms by considering additional Feynman diagrams contributing to the physical process under study. However, as argued in Ref. [1] the off-shell CMDM of the top quark is gauge-independent in the SM and the same is true for both the CMDM and CEDM in electroweak extension models. Also, as shown in Refs. [6, 7] there is little dependence of the top quark dipole form factors on q^2 over a large energy interval in the SM and some BSM theories. We will thus assume that both the real and absorptive parts of the CMDM and CEDM are constant and obtain bounds on the absorptive parts from the data on top quark production at the LHC.

The most recent analyses on top quark production assume that both CMDM and CEDM are purely real [47, 48]. In this work, we are interested in the study of the contributions of the absorptive parts of these dipole moments. Therefore, we consider that $\hat{\mu}_t$ and $\hat{d}_t$ are complex and calculate the following parton cross sections:

$$\hat{\sigma}_{q\bar{q}} \equiv \sigma(\overline{q}q \to t\bar{t}),$$
$$\hat{\sigma}_{gg} \equiv \sigma(gg \to t\bar{t}), \tag{5}$$

which apart from the SM contribution receive a new one from the Feynman diagrams of Fig. 4, where the large dot represents the anomalous CMDM and CEDM contributions.

After some algebra, we obtain the respective differential cross sections for general complex CMDM and CEDM:

$$
\frac{d\hat{\sigma}_{q\bar{q}}}{d\hat{t}} = \frac{\pi\alpha_s^2}{\hat{s}^2}\frac{8}{9}\left[\frac{1}{2} - v + z + 2\mathrm{Re}[\hat{\mu}_t] + \left(\mathrm{Re}[\hat{\mu}_t]^2 + \mathrm{Im}[\hat{\mu}_t]^2 - \mathrm{Re}[\hat{d}_t]^2 - \mathrm{Im}[\hat{d}_t]^2\right) \right.
$$
$$
\left. + \left(\mathrm{Re}[\hat{\mu}_t]^2 + \mathrm{Im}[\hat{\mu}_t]^2 + \mathrm{Re}[\hat{d}_t]^2 + \mathrm{Im}[\hat{d}_t]^2\right)\frac{v}{z}\right], \tag{6}
$$

and

$$
\frac{d\hat{\sigma}_{gg}}{d\hat{t}} = \frac{\pi\alpha_s^2}{\hat{s}^2}\frac{1}{12}\left[\left(\frac{4}{v} - 9\right)\left(\frac{1}{2} - v - 2z(1 - \frac{z}{v}) + 2\,\mathrm{Re}[\hat{\mu}_t]\right) + \frac{1}{8vz}\left[v\left(55\,\mathrm{Re}[\hat{d}_t]^2 + \mathrm{Re}[\hat{\mu}_t]^2(55 - 144z)\right)\right.\right.
$$
$$
+ z\left(4\,\mathrm{Re}[\hat{d}_t]^2 + 70\,\mathrm{Re}[\hat{\mu}_t]^2\right) + \frac{1}{vz}\left[-16v^3\left(4\left(\mathrm{Re}[\hat{\mu}_t]^2\mathrm{Im}[\hat{d}_t]^2 - 4\,\mathrm{Re}[\hat{\mu}_t]\,\mathrm{Im}[\hat{\mu}_t]\,\mathrm{Re}[\hat{d}_t]\,\mathrm{Im}[\hat{d}_t]\right.\right.\right.
$$
$$
+ \mathrm{Im}[\hat{\mu}_t]^2\,\mathrm{Re}[\hat{d}_t]^2\Big) + 9z\left(\mathrm{Im}[\hat{\mu}_t]^2 + \mathrm{Im}[\hat{d}_t]^2\right)\Big) + v^2z\Big(-512\,\mathrm{Re}[\hat{\mu}_t]\,\mathrm{Im}[\hat{\mu}_t]\,\mathrm{Re}[\hat{d}_t]\,\mathrm{Im}[\hat{d}_t]
$$
$$
+ \mathrm{Im}[\hat{d}_t]^2\left(16\,\mathrm{Re}[\hat{\mu}_t]\left(15\,\mathrm{Re}[\hat{\mu}_t] + 7\right) + 288z + 63\right) + 3\,\mathrm{Im}[\hat{\mu}_t]^2\left(80\,\mathrm{Re}[\hat{d}_t]^2 + 48z + 21\right)\Big)
$$
$$
- 2vz^2\Big(92\,\mathrm{Im}[\hat{\mu}_t]\,\mathrm{Re}[\hat{d}_t]\,\mathrm{Im}[\hat{d}_t] + \left(1 - 8\,\mathrm{Re}[\hat{d}_t]^2\right)\mathrm{Im}[\hat{\mu}_t]^2 + 2\,\mathrm{Im}[\hat{d}_t]^2\left(-\mathrm{Re}[\hat{\mu}_t]\left(4\,\mathrm{Re}[\hat{\mu}_t] + 41\right)\right.
$$
$$
+ 72z + 17\Big)\Big) + 128\,\mathrm{Im}[\hat{d}_t]^2z^3\Big] + \mathrm{Re}[\hat{\mu}_t]\left(\mathrm{Re}[\hat{\mu}_t]^2 + \mathrm{Im}[\hat{\mu}_t]^2 + \mathrm{Re}[\hat{d}_t]^2\right)\left(\frac{14}{z} - \frac{5}{2v}\right)
$$
$$
+ \left(\left(\mathrm{Re}[\hat{\mu}_t]^2 + \mathrm{Im}[\hat{\mu}_t]^2\right)^2 + 2\left(\mathrm{Re}[\hat{\mu}_t]^2\,\mathrm{Re}[\hat{d}_t]^2 + \mathrm{Im}[\hat{\mu}_t]^2\,\mathrm{Im}[\hat{d}_t]^2\right) + \left(\mathrm{Re}[\hat{d}_t]^2 + \mathrm{Im}[\hat{d}_t]^2\right)^2\right)
$$
$$
\times \left(-\frac{1}{z} + \frac{1}{v} + \frac{4v}{z^2}\right)\Big], \tag{7}
$$

where $\hat{s}$, $\hat{t}$ and $\hat{u}$ are the usual parton Mandelstam variables, and we introduced the definitions

$$z = \frac{m_t^2}{\hat{s}}, \tag{8}$$

$$v = \frac{1}{\hat{s}^2}(\hat{t} - m_t^2)(\hat{u} - m_t^2). \tag{9}$$

In the $t\bar{t}$ center of mass frame, the parameter $\hat{t}$ is related to the angle $\hat{\theta}$ between the momentum of the outgoing top quark and that of the incoming parton as

$$m_t^2 - \hat{t} = \frac{\hat{s}}{2}(1 - \beta\cos\hat{\theta}), \tag{10}$$

with $\beta = \sqrt{1 - 4z}$.

For $\hat{\mu}_t = \hat{d}_t = 0$, the above cross sections reduce to the known SM results [56] as expected. We also have verified that in the scenario with purely real CMDM and CEDM, Eq. (6) reproduces the result reported in Ref. [11, 12]. Nevertheless, in the same scenario we do not find agreement with our result for Eq. (7) and the one previously reported [11, 12], which apparently is incomplete as there is no agreement in the coefficients of $\hat{\mu}_t^2$ and $\hat{d}_t^2$.

4 Bounds on absorptive parts of the CMDM and CEDM of the top quark

We now turn to constrain the absorptive parts $\mathrm{Im}[\hat{\mu}_t]$ and $\mathrm{Im}[\hat{d}_t]$ via the LHC data on top quark pair production [47, 48, 57]. We follow a similar approach to that discussed in [22] and use a Monte Carlo simulation to obtain the theory predictions for the leading-order contribution to the $\sigma(pp \to t\bar{t})$ cross section. In order to compute the corresponding contributions from the top quark

Fig. 4 Feynman diagrams for the contribution to the parton cross sections $\hat{\sigma}_{q\bar{q}}$ and $\hat{\sigma}_{gg}$ at the leading order. Crossed diagrams are not shown. The large dot represents the anomalous couplings induced by the CMDM and CEDM. The SM tree-level contribution is obtained after replacing the anomalous $\bar{t}tg$ coupling by the SM one
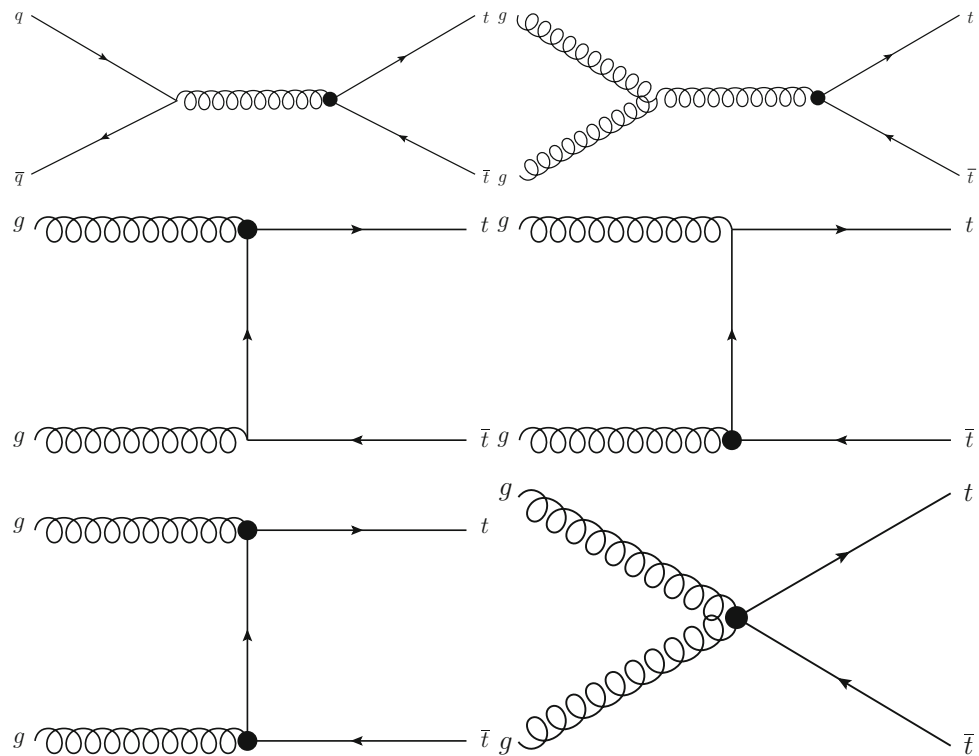
CMDM and CEDM, we use MadGraph5 [58], where the anomalous interactions of Eq. (2) were implemented with the help of FeynRules [59].

We will consider the most recent LHC results for top quark pair production at center-of-mass energy $\sqrt{s}$ =13 TeV. Therefore, we use the ATLAS cross section in the lepton plus jets channel [57]

$$\sigma_{\text{Exp}}(pp \to t\bar{t}) = (830 \pm 39) \quad \text{pb}, \tag{11}$$

whereas for the theoretical SM prediction we use [15, 60]

$$\sigma_{\text{Theo}}(pp \to t\bar{t}) = (831.8 \pm 43) \quad \text{pb}, \tag{12}$$

wherein both cases the errors have been added in quadrature. We will assume that the small deviation in $\sigma_{\text{Exp}}(pp \to t\bar{t})$ from the theoretical leading-order SM prediction $\sigma_{\text{Theo}}(pp \to t\bar{t})$ is due to the real and absorptive parts of the top quark CMDM and CEDM. While 90% (85%) of $\sigma(pp \to t\bar{t})$ arises dominantly from the partonic process $gg \to \bar{t}t$ at $\sqrt{s} = 14$ TeV ($\sqrt{s}$=7 TeV), the contribution of $\bar{t}tgg$ vertex has not been considered in the computation of (12) as it is a non-SM interaction. However, as observed in Eqs. (6) and (7), the dipole moments induce a deviation in $\sigma(pp \to t\bar{t})$. Thus, the top quark CMDM and CEDM may explain slight deviations from the SM prediction to $\bar{t}t$ production.

The ratio between the measured and predicted cross sections is

$$\mathcal{R} = \frac{\sigma_{\text{Exp}}(pp \to t\bar{t})}{\sigma_{\text{Theo}}(pp \to t\bar{t})} = 0.99 \pm 0.069. \tag{13}$$

Following Ref. [22], we will interpret the error of Eq. (13) as a window to BSM effects in top quark pair production and use it to set constraints on the absorptive parts of $\hat{\mu}_t$ and $\hat{d}_t$. As already mentioned, in the analysis of the CMS collaboration the CMDM and CEDM of the top quark were assumed to be real quantities. In Ref. [47], all the measurements are analyzed under a linearized approximation of the anomalous couplings [26], which parametrizes the non-SM interactions and include the $\bar{t}tgg$ vertex, though the dipole moments are not interpreted as complex quantities and thus the absorptive parts are not considered in the differential cross section used to study BSM effects. Also, in Ref. [48] the kinematic distribution used to obtain constraints on $\hat{\mu}_t$ and $\hat{d}_t$ are defined via Eqs. (6) and (7), though once again it was assumed that both the top quark CMDM and CEDM are real quantities. Thus, the effects of the absorptive parts have been never studied by the CMS collaboration, however, such consequences have a negligible effect on their analysis as the kinematic distributions measured at the LHC [20, 26] are strongly constrained [24, 27]. Below we will consider a similar approach to that followed in Refs. [22, 48] to obtain bounds on the absorptive parts of $\hat{\mu}_t$ and $\hat{d}_t$ by reinterpreting the LHC data. We will also show explicitly that the relevant kinematic distributions of $\bar{t}t$ production are not sensitive to the imaginary parts of the dipole moments, as already pointed out in Refs. [20, 23, 26].
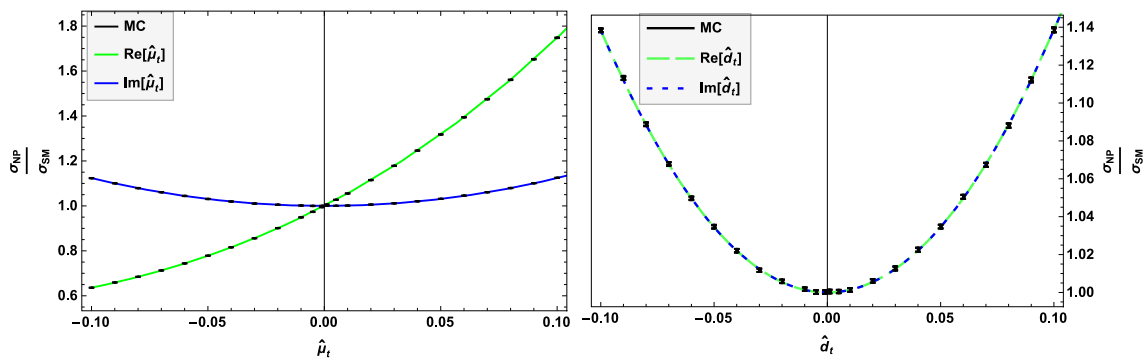
Fig. 5 Ratio $\mathcal{R} = \sigma_{\text{NP}}(pp \to t\bar{t})/\sigma_{\text{SM}}(pp \to t\bar{t})$ as a function of the real (green lines) and imaginary parts (blue lines) of the CMDM (left plot) and CEDM (right plot) of the top quark at $\sqrt{s} = 14$ TeV. The bars represent the MadGraph5 estimated errors and the solid lines are the best fit curves

To study the absorptive part of the top quark CMDM and CEDM, we proceed as follows: We first set $\hat{\mu}_t = \hat{d}_t = 0$ and obtain the SM cross section $\sigma_{\text{SM}}(pp \to t\bar{t})$, afterward we generate the new physics contribution $\sigma_{\text{NP}}(pp \to t\bar{t})$ for non-zero $\text{Re}[\hat{\mu}_t]$, whereas all the remaining parameters are set to zero. This procedure is repeated for each one of the $\text{Im}[\hat{\mu}_t]$, $\text{Re}[\hat{d}_t]$ and $\text{Im}[\hat{d}_t]$ parameters. All our event samples for the $pp \to \bar{t}t$ cross section are generated at $\sqrt{s} = 14$ TeV.

We show in Fig. 5 the ratio $\sigma_{\text{NP}}/\sigma_{\text{SM}}$ as a function of the real and absorptive parts of the CMDM (left plot) and CEDM (right plot), where the MadGraph5 estimated error is included. We plot the best-fit curves.

To fit the data of Fig. 5, we have not considered the interference terms of the real and absorptive parts of $\hat{\mu}_t$ and $\hat{d}_t$. Such an approach has been used in the past to study the implications of the top quark CMDM and CEDM in $t\bar{t}$ production [22, 29, 30]. Thus, from Eqs. (6) and (7) we observe that the ratio $\mathcal{R}$ is a fourth-order polynomial of the real and imaginary parts of $\hat{\mu}_t$ and $\hat{d}_t$, though there are only even powers of the absorptive parts. The expression obtained from the fit of Fig. 5 reads

$$\mathcal{R} \simeq 1 + 5.33\,\text{Re}[\hat{\mu}_t] + 19.14\,\text{Re}[\hat{\mu}_t]^2 + 21.98\,\text{Re}[\hat{\mu}_t]^3 + 5.78\,\text{Re}[\hat{\mu}_t]^4$$
$$+ 12.35\,\text{Im}[\hat{\mu}_t]^2 + 4.38\,\text{Im}[\hat{\mu}_t]^4 + 13.79\,\text{Re}[\hat{d}_t]^2 + 5.58\,\text{Re}[\hat{d}_t]^4$$
$$+ 13.78\,\text{Im}[\hat{d}_t]^2 + 6.15\,\text{Im}[\hat{d}_t]^4. \qquad (14)$$

We observe that the contributions of $\text{Im}[\hat{\mu}_t]$, $\text{Re}[\hat{d}_t]$ and $\text{Im}[\hat{d}_t]$ are of the same order and similar size, which is actually in accordance with Eq. (7). Moreover, $\mathcal{R}$ shows a similar dependence on the absorptive parts and $\text{Re}[\hat{d}_t]$, which makes it possible to obtain bounds on $\text{Im}[\hat{\mu}_t]$ and $\text{Im}[\hat{d}_t]$ following Refs. [22, 48], where limits on the real part of $\hat{d}_t$ are obtained using Eqs. (6), (7) and (14). We also note that the leading contribution to $\mathcal{R}$ arises from the linear term of $\text{Re}[\hat{\mu}_t]$ as the other dipole terms contribute quadratically at the lowest order and are thus more suppressed. The values predicted for the off-shell top quark CMDM are of the order of $10^{-2} - 10^{-3}$ in the SM [1], whereas the typical values predicted for the CEDM in some BSM theories are of the order of $10^{-19} - 10^{-20}$ [6]. Thus, the effects of the top quark dipole moments would hardly induce a significant deviation to the top quark production cross section.

To analyze the effects of the absorptive parts of the top quark dipole moments, we will proceed as follows. We fix the corresponding real parts using the CMS limits [47, 48], which allow us to constrain the absorptive parts $\text{Im}[\hat{\mu}_t]$ and $\text{Im}[\hat{d}_t]$ via Eqs. (14) and (13), with the error being attributed to the anomalous $\bar{t}tg$ contributions. In other words, we fix $\text{Re}[\hat{\mu}_t]$ and $\text{Re}[\hat{d}_t]$ to their current constraints and find the allowed area of $\text{Im}[\hat{\mu}_t]$ and $\text{Im}[\hat{d}_t]$ values. With this aim, we assume the following three scenarios:

– Scenario I: we use the lower bounds $\text{Re}[\hat{\mu}_t] = -0.014$ and $\text{Re}[\hat{d}_t] = -0.02$ reported in [47].
– Scenario II: we use the upper bounds $\text{Re}[\hat{\mu}_t] = 0.004$ and $\text{Re}[\hat{d}_t] = 0.012$ reported in [47].
– Scenario III: we use the value $\text{Re}[\hat{\mu}_t] = -0.024$ and the upper bound $\text{Re}[\hat{d}_t] = 0.03$ reported in [48].

We do not consider the scenario where $\text{Re}[\hat{d}_t]$ is set to its lower (negative) bound [48] as it yields similar bounds to those obtained in scenario III as $\mathcal{R}$ is an even function of $\text{Re}[\hat{d}_t]$. A similar situation arises for other possible scenarios, which yield bounds of a similar order of magnitude.

The allowed areas in the $\text{Im}[\hat{\mu}_t] - \text{Im}[\hat{d}_t]$ plane at the 95% C.L. are the concentric ellipses shown in Fig. 6 for the three scenarios discussed above. The corresponding bounds are: $|\text{Im}[\hat{\mu}_t]| \lesssim 0.127$ and $|\text{Im}[\hat{d}_t]| \lesssim 0.12$ in scenario I (blue solid lines); $|\text{Im}[\hat{\mu}_t]| \lesssim 0.139$ and $|\text{Im}[\hat{d}_t]| \lesssim 0.133$ in scenario III (green dot-dashed lines); and $|\text{Im}[\hat{\mu}_t]| \lesssim 0.094$ and $|\text{Im}[\hat{d}_t]| \lesssim 0.09$ in scenario II (orange dashed line). The latter scenario yields the intersected area allowed by the three scenarios, which means that the corresponding bounds are consistent with both CMS limits. Note that in both cases the bounds on the absorptive parts of $\hat{\mu}_t$ and $\hat{d}_t$ are quite similar, of the order of $10^{-1} - 10^{-2}$ at the 95% C.L.

Fig. 6 Allowed area at the 95% C.L. for the imaginary parts of the CMDM and CEDM of the top quark in the three scenarios discussed in the text for the corresponding real parts
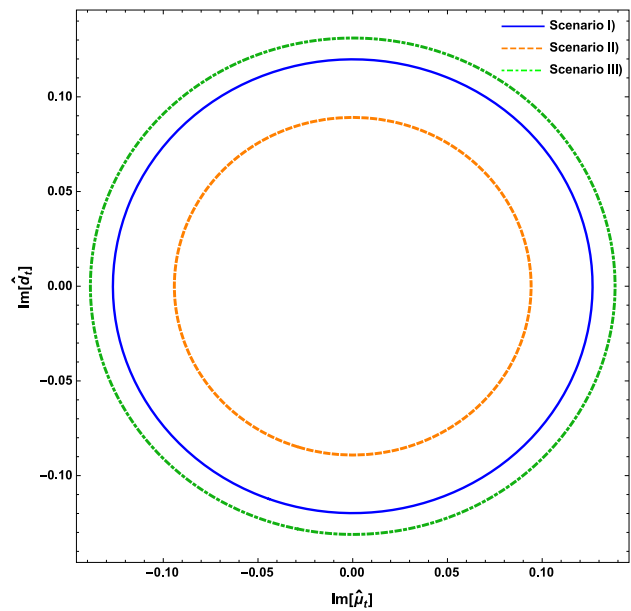
Fig. 7 Allowed area at the 95% C.L. for the imaginary parts of the CMDM and CEDM of the top quark at three different energies of the gluon transfer momentum
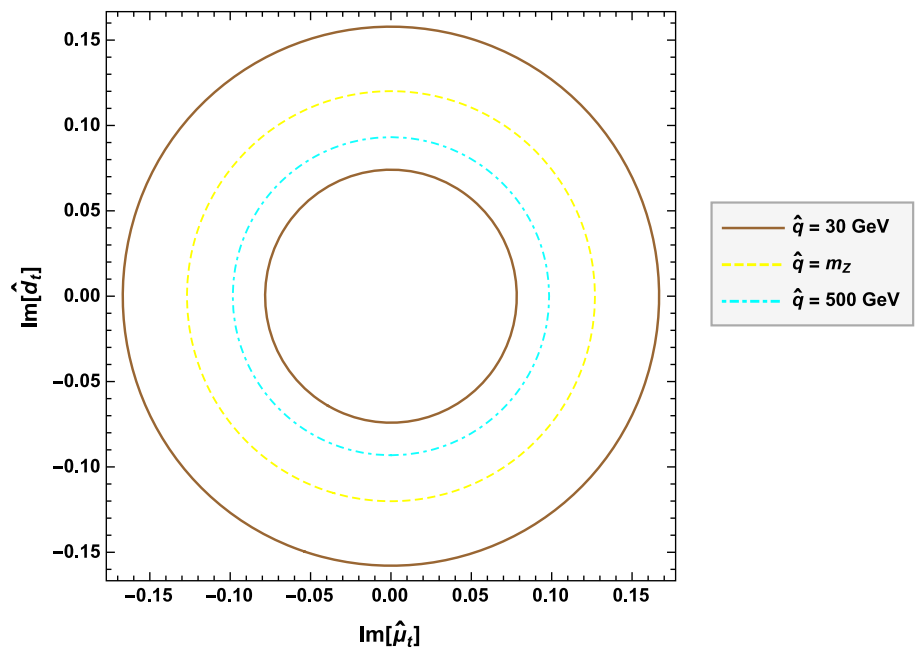
For completeness, we revisit the case where the gluon transfer four-momentum ($\hat{q} = \sqrt{q^2}$) dependence is considered for $\text{Re}[\hat{\mu}_t]$, which is possible using the expressions for $\hat{\mu}_t(q^2)$ reported in Ref. [1]. The real part of the CEDM is set as $\text{Re}[\hat{d}_t] = 0.01$ since there are not any analytic results for $\hat{d}_t(q^2)$. In Fig. 7, the allowed areas in the $\text{Im}[\hat{\mu}_t] - \text{Im}[\hat{d}_t]$ plane at the 95% C.L. for three different energies of $\hat{q}$ are shown. We note that at low energies ($\hat{q} = 30$ GeV) the bounds are slightly larger than scenario III, but they are still of the same order, whereas from $\hat{q} = m_Z$ the limits are similar to those found in Fig. 6. Thus, the bounds obtained by taking the real parts as constants are compatible with those where their dependence on $\hat{q}$ is considered. Especially, for energies above the Z boson mass both constraints are almost identical.

It is worth comparing our limits with the theoretical predictions of the SM and some BSM theories. In particular, for a transfer momentum in the interval $30 \text{ GeV} \leqslant \hat{q} \leqslant 1000 \text{ GeV}$, the SM prediction for the absorptive part of $\hat{\mu}_t(q^2)$ can be as large as 10^{-2} [1], which is close to our bounds. On the other hand, several BSM theories predict values for the absorptive part of $\hat{d}_t(q^2)$ of the order of 10^{-19}, which is far away from our bound.

We have also made the same analysis but including the interference terms of Eq. (7). Nonetheless, the obtained fit is still consistent with Eq. (14) and the bounds are similar to those of Fig. 6. Thus, the interference terms can be neglected as their contribution is not relevant.
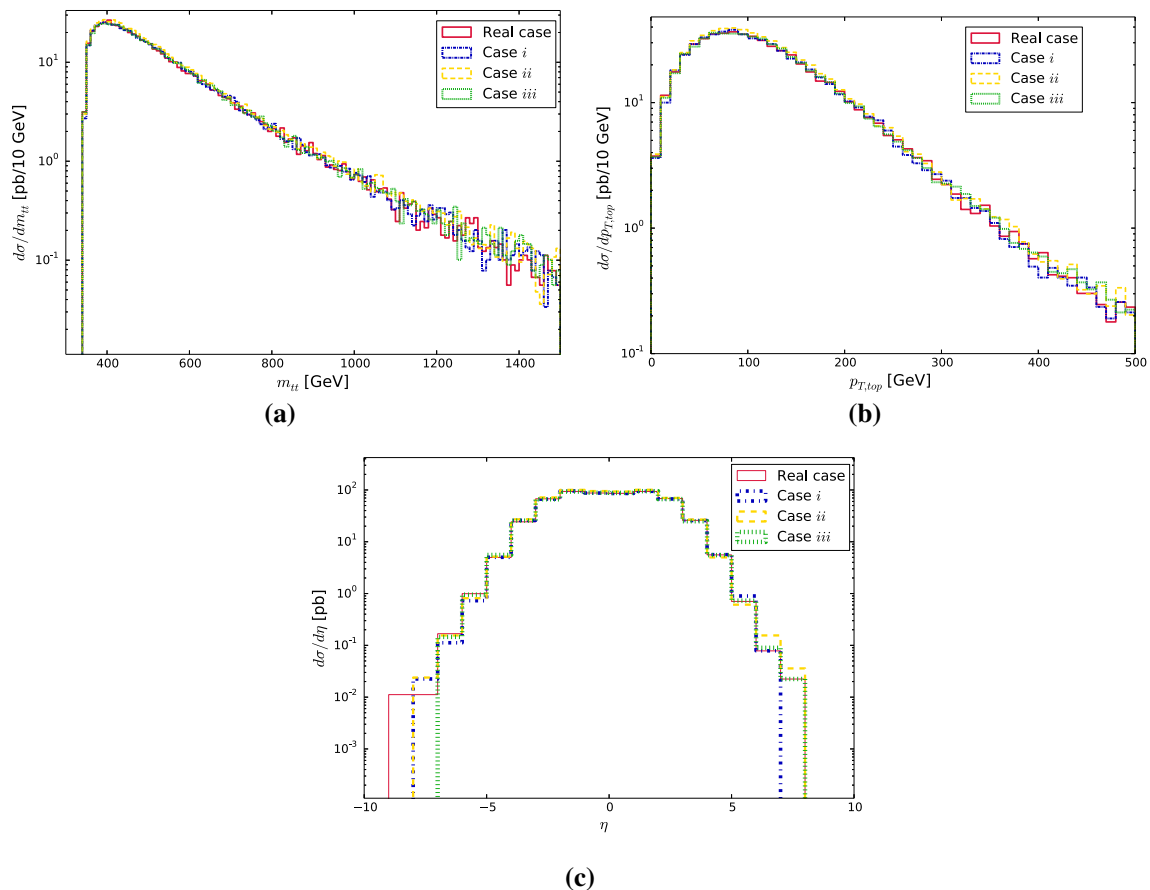
5 Kinematic distributions

The effects of $\text{Re}[\hat{\mu}_t]$ and $\text{Re}[\hat{d}_t]$ on top quark pair production have been analyzed in the past as some kinematic distributions can be sensitive to such parameters [9, 12, 28, 31]. On the other hand, to our knowledge the possible effects of the absorptive parts $\text{Im}[\hat{\mu}_t]$ and $\text{Im}[\hat{d}_t]$ have only been explored in Ref. [23] through the longitudinal t and $\bar{t}$ polarizations. Therefore, for completeness we will examine the possibility that the differential cross sections for top quark pair production could be sensitive to the absorptive parts of the top quark CMDM and CEDM, such implications are supposed to be unobservable [20, 26]; nonetheless, it has been never shown explicitly. To this end, we use the CMS constraints on the real parts of the top quark dipole form factors ($\text{Re}[\hat{\mu}_t] = -0.014$ and $\text{Re}[\hat{d}_t] = 0.01$) and analyze any possible deviation in the kinematic distributions of top quark production when both dipole moments develop an absorptive part. We consider the following three cases for $\text{Im}[\hat{\mu}_t]$ and $\text{Im}[\hat{d}_t]$:

  (i) $\text{Im}[\hat{\mu}_t] = \text{Im}[\hat{d}_t] = 0.01$.
  (ii) $\text{Im}[\hat{\mu}_t] = \text{Im}[\hat{d}_t] = 0.05$.
  (iii) $\text{Im}[\hat{\mu}_t] = 0.01$ and $\text{Im}[\hat{d}_t] = -0.01$.

We consider such values as they are consistent with the SM prediction for the CMDM and the constraints of Sect. 4. Scenarios (i) and (ii) allow us to explore the possibility that the kinematic distributions can be sensitive to small changes in the absorptive terms, whereas scenario (iii) allows us to test the effect of a flip of sign. For the graphical analysis, we use MADANALYSIS 5 [61].

In Fig. 8a and b, we show the kinematic distributions of the $t\bar{t}$ invariant mass and the top quark transverse momentum in the scenarios discussed above. It is observed that there is no considerable distinction between the kinematic distributions obtained in the general case with complex top quark dipole form factors and those obtained in the scenario in which they are purely real. This was also observed in the case where the contributions of the real part of the top quark dipole moments are compared with the SM leading-order contribution [19, 28]. A similar situation occurs for the kinematic distribution of the rapidity η, which is shown in Fig. 8c.

Fig. 8 Invariant mass (**a**), top quark transverse momentum (**b**) and rapidity (**c**) kinematic distributions for top quark pair production at the LHC at $\sqrt{s} = 14$ TeV in the three scenarios discussed in the text for the absorptive parts of $\hat{\mu}_t$ and $\hat{d}_t$

We have also examined the sensitivity of the forward–backward (FB) asymmetry to the CMDM and CEDM in top quark pair production at the LHC, which is possible at the leading order in some models [19, 62], whereas in the SM there is only a significant deviation up to next-to-leading order [62]. Unfortunately, Eqs. (6) and (7) cannot be expressed as a linear combination of $\cos \theta$ via Eq. (10). Thus, a deviation to the FB asymmetry at the leading order is not possible [63]. However, other asymmetries could be sensitive to the CMDM and CEDM of the top quark, as shown in Ref. [22, 23]. In summary, all the kinematic distributions studied here show no significant deviation from leading-order contribution to top quark pair production arising from the real and absorptive parts of the top quark dipole form factors.

6 Conclusions

The off-shell CMDM and CEDM of quarks have become a topic of interest recently [1, 2]. However, the study of their absorptive (imaginary) parts remains almost unexplored. In this work, we have obtained bounds on the new physics contributions to the absorptive parts of the off-shell top quark CMDM and CEDM via the experimental data of top quark pair production at the LHC, which to our knowledge are the first limits of this kind. We present explicit expressions for the corresponding differential parton cross sections considering complex CMDM and CEDM, which have also been calculated for the first time. We point out that there is a disagreement between our result for the $gg \to t\bar{t}$ differential cross section and the expression previously reported in the scenario where only the real part of the top quark dipole form factors are considered [11, 12]. Our bounds for the absorptive parts were obtained using the most recent data for the top quark CMDM and CEDM reported by the CMS collaboration [47, 48]. It was found that the upper bound on the absorptive parts of both dipole moments are of order $10^{-1} - 10^{-2}$. In particular, values of order 10^{-2} are consistent with all the CMS results. We also note that our bound on $\mathrm{Im}[\hat{\mu}_t]$ is consistent with the SM prediction for the absorptive part of $\hat{\mu}_t$, which is of order $10^{-2} - 10^{-3}$ [1, 2]. On the other hand, in some BSM theories the absorptive part of the CEDM is of the order of 10^{-19} [6], which seems well beyond the experimental reach. Our limits could be useful to constrain the parameter space of BSM theories and are consistent with the case where the gluon transfer four-momentum ($\hat{q}$) dependence is considered for the real part of the top quark CMDM.

We also explored the possibility that several kinematic distributions for top quark pair production at the LHC can be sensitive to the absorptive parts of the CMDM and CEDM, but we find that there are no significant deviation from the scenario where the CMDM and CEDM are purely real. In fact, even in the case of real CMDM and CEDM, there is no significant deviation from the leading-order SM contribution as discussed previously [19, 28].

Data Availability Statement The datasets generated during and/or analyzed during the current study are available from the corresponding author on reasonable request. This manuscript has associated data in a data repository. [Authors' comment: All data included in this manuscript are available upon request by contacting with the corresponding author.]

References

1. A.I. Hernández-Juárez, A. Moyotl, G. Tavares-Velasco, New estimate of the chromomagnetic dipole moment of quarks in the standard model. Eur. Phys. J. Plus **136**(2), 262 (2021)
2. J.I. Aranda, T. Cisneros-Pérez, J. Montaño, B. Quezadas-Vivian, F. Ramírez-Zavaleta, E.S. Tututi, Revisiting the top quark chromomagnetic dipole moment in the SM. Eur. Phys. J. Plus **136**(2), 164 (2021)
3. R. Martinez, M.A. Perez, N. Poveda, Chromomagnetic dipole moment of the top quark revisited. Eur. Phys. J. C **53**, 221–230 (2008)
4. R. Gaitan, E.A. Garces, J.H. Montes de Oca, R. Martinez, Top quark chromoelectric and chromomagnetic dipole moments in a two Higgs doublet model with CP violation. Phys. Rev. D **92**(9), 094025 (2015)
5. A.I. Hernández-Juárez, A. Moyotl, G. Tavares-Velasco, Chromomagnetic and chromoelectric dipole moments of the top quark in the fourth-generation THDM. Phys. Rev. D **98**(3), 035040 (2018)
6. A.I. Hernández-Juárez, A. Moyotl, G. Tavares-Velasco, Chromomagnetic and chromoelectric dipole moments of quarks in the reduced 331 model. Chin. Phys. C **45**(11), 113101 (2021)
7. J.I. Aranda, D. Espinosa-Gómez, J. Montaño, B. Quezadas-Vivian, F. Ramírez-Zavaleta, E.S. Tututi, Flavor violation in chromo- and electromagnetic dipole moments induced by Z' gauge bosons and a brief revisit of the standard model. Phys. Rev. D **98**(11), 116003 (2018)
8. A. Czarnecki, B. Krause, Neutron electric dipole moment in the standard model: valence quark contributions. Phys. Rev. Lett. **78**, 4339–4342 (1997)
9. D. Atwood, A. Kagan, T.G. Rizzo, Constraining anomalous top quark couplings at the Tevatron. Phys. Rev. D **52**, 6264–6270 (1995)
10. E.H. Simmons, P.L. Cho, Anomalous gluon self-interactions and $t\bar{t}$ production. AIP Conf. Proc. **350**, 323–334 (1995)
11. P. Haberl, O. Nachtmann, A. Wilch, Top production in hadron hadron collisions and anomalous top - gluon couplings. Phys. Rev. D **53**, 4875–4885 (1996)
12. K. Cheung, Probing the chromoelectric and chromomagnetic dipole moments of the top quark at hadronic colliders. Phys. Rev. D **53**, 3604–3615 (1996)
13. S.Y. Choi, C.S. Kim, J. Lee, T - odd gluon - top quark effective couplings at the CERN large hadron collider. Phys. Lett. B **415**, 67–74 (1997)
14. K.I. Hikasa, K. Whisnant, J.M. Yang, B.L. Young, Probing anomalous top quark interactions at the Fermilab Tevatron collider. Phys. Rev. D **58**, 114003 (1998)

15. M. Czakon, A. Mitov, Inclusive heavy flavor hadroproduction in NLO QCD: the exact analytic result. Nucl. Phys. B **824**, 111–135 (2010)
16. O. Antipin, G. Valencia, T-odd correlations from CP violating anomalous top-quark couplings revisited. Phys. Rev. D **79**, 013013 (2009)
17. S.K. Gupta, G. Valencia, CP-odd correlations using jet momenta from $t\bar{t}$ events at the Tevatron. Phys. Rev. D **81**, 034013 (2010)
18. C. Zhang, S. Willenbrock, Effective-field-theory approach to top-quark production and decay. Phys. Rev. D **83**, 034006 (2011)
19. C. Degrande, J.-M. Gerard, C. Grojean, F. Maltoni, G. Servant, Non-resonant new physics in top pair production at hadron colliders. JHEP **03**, 125 (2011)
20. M. Baumgart, B. Tweedie, A new twist on top quark spin correlations. JHEP **03**, 117 (2013)
21. C. Englert, A. Freitas, M. Spira, P.M. Zerwas, Constraining the intrinsic structure of top-quarks. Phys. Lett. B **721**, 261–268 (2013)
22. A. Hayreter, G. Valencia, Constraints on anomalous color dipole operators from Higgs boson production at the LHC. Phys. Rev. D **88**, 034033 (2013)
23. W. Bernreuther and Z.-G. Si, Top quark spin correlations and polarization at the LHC: standard model predictions and effects of anomalous top chromo moments. *Phys. Lett. B*, 725:115–122, 2013. [Erratum: Phys. Lett. B 744, 413–413 (2015)]
24. M. Fabbrichesi, M. Pinamonti, A. Tonero, Limits on anomalous top quark gauge couplings from Tevatron and LHC data. Eur. Phys. J. C **74**(12), 3193 (2014)
25. J.A. Aguilar-Saavedra, B. Fuks, M.L. Mangano, Pinning down top dipole moments with ultra-boosted tops. Phys. Rev. D **91**, 094021 (2015)
26. W. Bernreuther, D. Heisler, Z.-G. Si, A set of top quark spin correlation and polarization observables for the LHC: standard model predictions and new physics contributions. JHEP **12**, 026 (2015)
27. Q.-H. Cao, B. Yan, Y. Jiang-Hao, C. Zhang, A general analysis of Wtb anomalous couplings. Chin. Phys. C **41**(6), 063101 (2017)
28. D. Barducci, M. Fabbrichesi, A. Tonero, Constraints on top quark nonstandard interactions from Higgs and $t\bar{t}$ production cross sections. Phys. Rev. D **96**(7), 075022 (2017)
29. M. Malekhosseini, M. Ghominejad, H. Khanpour, M.M. Najafabadi, Constraining top quark flavor violation and dipole moments through three and four-top quark productions at the LHC. Phys. Rev. D **98**(9), 095001 (2018)
30. C. Englert, D. Goncalves, M. Spannowsky, Nonstandard top substructure. Phys. Rev. D **89**(7), 074038 (2014)
31. D.B. Franzosi, C. Zhang, Probing the top-quark chromomagnetic dipole moment at next-to-leading order in QCD. Phys. Rev. D **91**(11), 114010 (2015)
32. D. Barducci et al, Interpreting top-quark LHC measurements in the standard-model effective field theory. 2 (2018)
33. G.L. Kane, G.A. Ladinsky, C.P. Yuan, Using the top quark for testing standard model polarization and CP predictions. Phys. Rev. D **45**, 124–141 (1992)
34. D. Atwood, A. Aeppli, A. Soni, Extracting anomalous gluon - top effective couplings at the supercolliders. Phys. Rev. Lett. **69**, 2754–2757 (1992)
35. B. Grzadkowski, B. Lampe, K.J. Abraham, CP violation, top quarks and the Tevatron upgrade. Phys. Lett. B **415**, 193–199 (1997)
36. B. Lampe, New interactions in top quark production and decay at the Tevatron upgrade. Phys. Lett. B **415**, 63–66 (1997)
37. J.M. Yang, B.-L. Young, Dimension-six CP violating operators of the third family quarks and their effects at colliders. Phys. Rev. D **56**, 5907–5918 (1997)
38. S. Tsuno, I. Nakano, Y. Sumino, R. Tanaka, Search for anomalous couplings in top decay at hadron colliders. Phys. Rev. D **73**, 054011 (2006)
39. Z. Hioki, K. Ohkuma, Search for anomalous top-gluon couplings at LHC revisited. Eur. Phys. J. C **65**, 127–135 (2010)
40. S.K. Gupta, A.S. Mete, G. Valencia, CP violating anomalous top-quark couplings at the LHC. Phys. Rev. D **80**, 034013 (2009)
41. Z. Hioki, K. Ohkuma, Addendum to: search for anomalous top-gluon couplings at LHC revisited. Eur. Phys. J. C **71**, 1535 (2011)
42. Z. Hioki, K. Ohkuma, Exploring anomalous top interactions via the final lepton in $t\bar{t}$ productions/decays at hadron colliders. Phys. Rev. D **83**, 114045 (2011)
43. J.F. Kamenik, M. Papucci, A. Weiler, Constraining the dipole moments of the top quark. *Phys. Rev. D*, 85:071501, 2012. [Erratum: Phys. Rev. D 88, 039903 (2013)]
44. Z. Hioki, K. Ohkuma, Optimal-observable analysis of possible non-standard top-quark couplings in $pp -> t\bar{t}X -> l^{+}X'$. Phys. Lett. B **716**, 310–315 (2012)
45. Z. Hioki, K. Ohkuma, Latest constraint on nonstandard top-gluon couplings at hadron colliders and its future prospect. Phys. Rev. D **88**, 017503 (2013)
46. R.M. Abraham, D. Gonçalves, T. Han, S.C.I. Leung, H. Qin, Directly probing the Higgs-top coupling at high scales. Phys. Lett. B **825**, 136839 (2022)
47. A.M. Sirunyan et al., Measurement of the top quark polarization and $t\bar{t}$ spin correlations using dilepton final states in proton-proton collisions at $\sqrt{s} = 13$ TeV. Phys. Rev. D **100**(7), 072002 (2019)
48. A.M. Sirunyan et al., Measurement of the top quark forward-backward production asymmetry and the anomalous chromoelectric and chromomagnetic moments in pp collisions at $\sqrt{s} = 13$ TeV. JHEP **06**, 146 (2020)
49. C. Arzt, M.B. Einhorn, J. Wudka, Patterns of deviation from the standard model. Nucl. Phys. B **433**, 41–66 (1995)
50. J.A. Aguilar-Saavedra, A Minimal set of top-Higgs anomalous couplings. Nucl. Phys. B **821**, 215–227 (2009)
51. M. Nowakowski, E.A. Paschos, J.M. Rodriguez, All electromagnetic form-factors. Eur. J. Phys **26**, 545–560 (2005)
52. A.I. Davydychev, P. Osland, L. Saks, Quark gluon vertex in arbitrary gauge and dimension. Phys. Rev. D **63**, 014022 (2001)
53. U. Baur, E.L. Berger, Probing the weak boson sector in $Z\gamma$ production at hadron colliders. Phys. Rev. D **47**, 4889–4904 (1993)
54. R.E. Cutkosky, Singularities and discontinuities of Feynman amplitudes. J. Math. Phys. **1**(5), 429–433 (1960)
55. Y. Zhou, Imaginary part of Feynman amplitude, cutting rules and optical theorem. 12 (2004)
56. M. Gluck, J.F. Owens, E. Reya, Gluon contribution to hadronic J/psi production. Phys. Rev. D **17**, 2324 (1978)
57. G. Aad et al., Measurement of the $t\bar{t}$ production cross-section in the lepton+jets channel at $\sqrt{s} = 13$ TeV with the ATLAS experiment. Phys. Lett. B **810**, 135797 (2020)
58. J. Alwall, R. Frederix, S. Frixione, V. Hirschi, F. Maltoni, O. Mattelaer, H.S. Shao, T. Stelzer, P. Torrielli, M. Zaro, The automated computation of tree-level and next-to-leading order differential cross sections, and their matching to parton shower simulations. JHEP **07**, 079 (2014)
59. A. Alloul, N.D. Christensen, C. Degrande, C. Duhr, B. Fuks, FeynRules 2.0 - a complete toolbox for tree-level phenomenology. Comput. Phys. Commun. **185**, 2250–2300 (2014)
60. P.A. Zyla et al., Review of particle physics. PTEP **2020**(8), 083C01 (2020)
61. E. Conte, B. Fuks, G. Serret, MadAnalysis 5, a user-friendly framework for collider phenomenology. Comput. Phys. Commun. **184**, 222–256 (2013)
62. I. Dorsner, S. Fajfer, J.F. Kamenik, N. Kosnik, Light colored scalars from grand unification and the forward-backward asymmetry in t t-bar production. Phys. Rev. D **81**, 055009 (2010)
63. P.H. Frampton, J. Shu, K. Wang, Axigluon as possible explanation for p anti-p –> t anti-t forward-backward asymmetry. Phys. Lett. B **683**, 294–297 (2010)